



MHD Double Diffusive Convection of Al₂O₃-Water Nanofluid in a Porous Medium Filled an Annular Space inside Two Vertical Concentric Cylinders with Discrete Heat Flux

M. Sammouda^{1†} and K. Gueraoui²

¹ Polydisciplinary Faculty, Sultan Moulay Slimane University, BP. 592, 23000 - Béni Mellal, Morocco

² Faculty of Sciences, Mohammed V University, B.P. 1014 RP, Rabat-Morocco

† Corresponding Author Email: sammouda.mohammed@gmail.com

(Received November 21, 2020; accepted February 27, 2021)

ABSTRACT

The magnetoconvection phenomenon of a double diffusive free convection in an annular porous space inside two concentric cylinders saturated by a (Al₂O₃, water) nanofluid has been investigated in the current study. The transport equations for vorticity, energy and concentration as well as stream function are solved using the finite difference method. At lower temperatures and concentrations, the outer cylinder is sustained, the discrete heat flux with the unheated adiabatic portions as well as the higher concentrations are imposed in the inside walls of the central cylinder. The base walls are insulated and impermeable. In the vertical direction, external magnetic field (MF) with uniform intensity is applied. The results of the obtained numerical simulation are presented to exhibit the consequences of various numbers such: Rayleigh Ra_{Th}, Hartmann Ha, Buoyancy forces ratio N and the solid nanoparticles (NPs) volume fraction ϕ on the pattern of the nanofluid flow and the transferred mass and thermal energy in the active wall. It is noted that the transferred mass and thermal flux in the active wall augments as the Ra_{Th} and N augments. The thermal energy transferred augments with the growth of ϕ , while the transferred mass in the active wall decreases. The greater magnetism declines the rate of the mass and thermal energy transport in the active wall.

Keywords: Nanofluid, MHD double-diffusive convection, Heat flux, Porous media, Cylindrical annulus, Finite-difference method.

NOMENCLATURE

AR_r	Aspect ratio (Radius)	Sh_{local}	Sherwood number local
B	Magnetic field	$Sh_{average}$	Sherwood number average
C	Concentration	Greek symbols	
C_F	Constant of Forchheimer	Ψ	Stream function
Da	Darcy number	Ω	Vorticity
g	Gravity acceleration	β_{Th}	Coefficient of thermal expansion
Ha	Hartmann number	β_{SL}	Coefficient of solutal expansion
K	Porous medium permeability	γ	Dimensionless length of heat flux
k^*	Thermal diffusivity of porous medium	ρ	Density
k_{Th}, k_{SL}	Thermal and solutal diffusivity	λ^*	Thermal conductivity of porous medium
Le	Number of Lewis	λ	Thermal conductivity
N	Buoyancy ratio	μ^*	Effective dynamic viscosity
N_r, N_z	Number of grid in radial and axial direction	μ	Dynamic viscosity
Nu_{local}	Number of Nusselt local	ε	Porosity
$Nu_{average}$	Number of Nusselt average	ϕ	Nanoparticles volume fraction
Pr	Prandtl number	σ	Electric conductivity
P	Pressure	ν	Kinematic viscosity
Q	Heat flux	Subscripts	
Ra_{Th}	Thermal Rayleigh number	nrf	Nanofluid
Ra_{SL}	Solutal Rayleigh number	fl	Fluid

r,z	Radius and height of cylinder	pr	Nanoparticles
T	Cylindrical coordinates	S	Solid porous matrix
V	Temperature		
U,W	Darcy velocity		
	Dimensionless velocity components		

1. INTRODUCTION

The phenomenon of double diffusive natural convection through porous media becomes the main focus of several researchers due to its presence in lots of industrial and technical applications, such as metallurgy, electro-chemistry, biology, geophysical systems and chemical processes. It will be interesting to precise that this phenomenon refers to buoyancy driven fluid flow under a combined effect of gradients of concentrations and temperatures. It occurs when the competitiveness between stabilizing and destabilizing buoyancy is induced by a difference in the diffusivity of each source.

Various experimental, analytical and numerical studies have been reported during the last few decades to study the phenomenon of the transport of mass and the thermal energy by combining the gradients of temperatures and concentrations by (Kramer *et al.* 2007; Sivasanka and Kandaswami 2008; Luzia *et al.* 2009; Cheng 2009; Sammouda *et al.* 2013; Muthamilselvan *et al.* 2018; Shahid and Altamush 2016; Saini and Sharma 2018). Ghorayeb and Mojtabi (1997) studied the double diffusive natural convection in vertical enclosures. They investigate the effect of aspect ratios and Lewis numbers on the fluid flow pattern and heat and mass transfer. Jagadeesha *et al.* (2015) investigated the double-diffusive convection in an inclined parallelogram enclosure. They reported that the inclination angle of the enclosure influence significantly the convective flow, heat and mass transfer characteristics. Tapas *et al.* (2013) investigated the effect of uniform and non-uniform heating of walls on double-diffusive natural convection in a lid-driven square enclosure. Jagadeesha *et al.* (2017) studied double diffusive magneto-convection in an inclined porous parallelogram enclosure. They found that the fluid flow pattern, thermal and solute distributions, as well as the resulting heat and mass transfer rates are significantly influenced by the cavity inclination angle and the applied magnetic field. Hemmat Esfe *et al.* (2015) studied the phenomenon of mixed convection of water/ Al_2O_3 nanofluid in a square enclosure. A rectangular shaped hot obstacle is located on the bottom wall of the enclosure. They found that the thermal energy transferred is controlled by the height of the hot obstacle and the NPs volume fraction.

The effect of magnetic field on the dynamics of nanofluids and the rate of heat and mass transfer in enclosures by natural convective heat transfer or by the combination of temperature and concentration gradients has been carried out by many researchers. Mebarek-Oudina and Bessaih (2016) investigated the oscillatory of MHD natural convection of liquid metal between upturned coaxial cylinders. They concluded that the variation of direction and

magnitude of implemented magnetic field can manage the transition stability and thermal energy transport rate. Mahapatra *et al.* (2018) studied numerically the consequence of MF on thermosolutal convection in a trapezoidal enclosure packed with nanofluid. They found that the mass transfer ratio is more effective in nanofluid than the base fluid. Mebarek-Oudina *et al.* (2020) presented a numerical study of MHD natural convection in an upright porous cylindrical annulus charged with magnetized nanoliquids. They conclude that the larger magnetism reduces the mass and thermal energy transport rate. Rujda and Mahapatra (2019) presented a numerical simulation of double diffusive natural convection of a nanofluid contained in a wavy-walled enclosure with a center heater under the influence of uniform vertical MF. They found that the heat and the mass transport rate increases as Rayleigh number and volumetric fraction of NPs increase and decreases with the increase in Hartmann number.

Yadav *et al.* (2016) investigated the MHD convection of electrically conducting Al_2O_3 -water and Cu-water nanofluid subjected to new set, more realistic, boundary condition for NPs volume fraction. They found that the onset of convective flow is affected by this realistic boundary condition. Yadav *et al.* (2017) studied the rotation effect on the onset of natural convection in a porous medium with internal heating and with different thermal and dynamic boundary condition. They concluded that the onset of convection is inhibited with the increase of the rotation parameter, so the rotation has a stabilization effect on the system. Yadav and Wang (2018) examined the onset on natural convection in Darcy porous layer saturated by non-Newtonian nanofluid with non-uniform internal source. They carried out that the thermal energy transferred across the porous medium increases and the stability of the system is affected by the NPs parameters as the internal source parameter increases. Dat *et al.* (2019) investigated the MHD convection in a porous layer with different NPs shape with the aid of CVFEM modeling. They concluded that the conductive transfer of thermal energy may be prevailing over the convection by increasing the intensity of the magnetism. Trung *et al.* (2019) presented the MHD on nanofluid free convection with different NPs shape in a Darcy porous medium with hot elliptic source. They carried the radiation source enhance the thermal energy transferred and the magnetism decline the heat transfer. Fakour *et al.* (2017) studied numerically with the aid of LSM method, the MHD nanofluid flow in a channel with the presence of MF and the walls of the channel are considered permeable. They found that the applied MF reduces the fluid flow intensity which leads to an increase in maximum temperature. Sajad *et al.* (2020) investigated

numerically, in square cavity, the MHD nanofluid mixed convection in the presence of vortex generators inside the enclosure with different organization. They found that the thermal energy transport increases as the Ha number decreases and the NPs volume fraction increases.

Mohebbi *et al.* (2019) studied numerically, with the aid of LBM, the heat transfer by free convection in a corrugated \cap shaped enclosure using hybrid nanofluid. They found that the consequence of hybrid nanofluid on heat transfer is significant than nanofluid. Ahmad *et al.* (2020) analyzed the nanofluid flow in porous media with a gyrotactic microorganisms dispersed in the nanofluid taking into account the chemical reaction. They concluded that the gyrotactic microorganisms added to the nanofluid improve its stability. Sohankar *et al.* (2019) provided a numerical investigation of heat transfer by forced convection in a rotating \cup shaped microchannel by using water and water/alumina nanofluid. They found that using NPs in the base fluid provides a significant improvement in the thermal energy transport.

After literature survey, one can conclude the absence of investigation showing the influence of magnetic field on the MHD double diffusive convection in an annular porous space created by two concentric vertical cylinders and subjected to a discrete heat flux. In the present work, we investigate the phenomenon of MHD double diffusive convection in an annular porous space inside two concentric vertical cylinders saturated by Al_2O_3 -water of a Newtonian nanofluid and subjected to a discrete heat flux placed on the inner cylinder.

2. MATHEMATICAL FORMULATION

Let us consider a Newtonian incompressible nanofluid saturated a porous matrix enclosed in an annular space inside two concentric cylinders Fig. 1. The discrete heat flux with the unheated adiabatic portions as well as the higher concentrations are imposed in the inside walls of the central cylinder. The base walls are insulated and impermeable. In the vertical direction, external MF with uniform intensity is applied. Under these assumptions, the governing equations in two-dimensional nanofluid double-diffusive magnetoconvection flow, with the formulation (vorticity-stream function) under the approximation of Boussinesq (Kaviany 1995; Donald *et al.* 2006; Sammouda *et al.* 2011) and in dimensionless form by using the following parameter;

$$R_i, T_{ref} = \frac{QR}{\lambda_{fl}}, \Delta C_{ref} = C_H - C_B, C_{ref} = C_B, \frac{k_{nmf}^*}{R}, \frac{R^2}{k_{nmf}^*}$$

For length, temperature, velocity and time, are defined as follows:

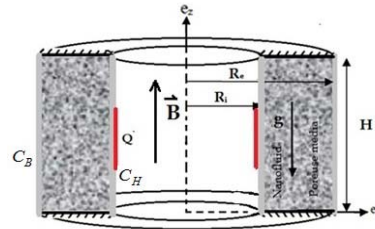


Fig. 1. Schematic for the physical model

$$\frac{1}{r} \frac{\partial(rU)}{\partial r} + \frac{\partial W}{\partial z} = 0 \tag{1}$$

$$\frac{\partial(UT)}{\partial r} + \frac{\partial(WT)}{\partial z} + \frac{UT}{r} = \frac{\partial^2 T}{\partial r^2} + \frac{\partial^2 T}{\partial z^2} + \frac{1}{r} \frac{\partial T}{\partial r} \tag{2}$$

$$\frac{\partial(UC)}{\partial r} + \frac{\partial(WC)}{\partial z} + \frac{UC}{r} = \frac{1}{Le} \left(\frac{\partial^2 T}{\partial r^2} + \frac{\partial^2 T}{\partial z^2} + \frac{1}{r} \frac{\partial T}{\partial r} \right) \tag{3}$$

$$\frac{1}{\varepsilon^2} \left(\frac{\partial(U\Omega)}{\partial r} + \frac{\partial(W\Omega)}{\partial z} \right) = \left(-\bar{\lambda} \Sigma \frac{Pr_{fl}}{Da} - \bar{\lambda} \Lambda \Sigma \frac{Pr_{fl}}{r^2} - \frac{C_F}{\sqrt{Da}} |\vec{V}| \right) \Omega + \bar{\lambda} \Lambda \Sigma Pr_{fl} \left(\frac{\partial^2 \Omega}{\partial r^2} + \frac{\partial^2 \Omega}{\partial z^2} + \frac{1}{r} \frac{\partial \Omega}{\partial r} \right) - \bar{\lambda}^2 \Gamma Ra_{Th} Pr_{fl} \left(\frac{\partial T}{\partial r} + \frac{\bar{\Gamma}}{\Gamma} N \frac{\partial C}{\partial r} \right) \tag{4}$$

$$-\frac{C_F}{\sqrt{Da}} \left(U \frac{\partial |\vec{V}|}{\partial z} - W \frac{\partial |\vec{V}|}{\partial r} \right) - \bar{\lambda} \frac{\sigma_{nf}}{\sigma_f} Ha^2 Pr_{fl} \frac{\Sigma}{(1-\phi)^{-2.5}} \frac{\partial U}{\partial z}$$

$$\frac{1}{r} \left(\frac{\partial^2 \Psi}{\partial r^2} + \frac{\partial^2 \Psi}{\partial z^2} - \frac{1}{r} \frac{\partial \Psi}{\partial r} \right) = \Omega \tag{5}$$

$$U = \frac{1}{r} \left(\frac{\partial \Psi}{\partial z} \right), \quad W = -\frac{1}{r} \left(\frac{\partial \Psi}{\partial r} \right) \tag{6}$$

Where:

$$\Gamma = \frac{\left((1-\phi) + \phi \frac{(\rho\beta_{Th})_{pr}}{(\rho\beta_{Th})_{fl}} \right)}{\left((1-\phi) + \phi \frac{\rho_{pr}}{\rho_{fl}} \right) \left(\frac{\lambda_{nmf}}{\lambda_{fl}} \frac{(\rho C)_{pr}}{(\rho C)_{fl}} \right)} \tag{7}$$

$$\bar{\Gamma} = \frac{\left((1-\phi) + \phi \frac{(\rho\beta_{SL})_{pr}}{(\rho\beta_{SL})_{fl}} \right)}{\left((1-\phi) + \phi \frac{\rho_{pr}}{\rho_{fl}} \right) \left(\frac{\lambda_{nmf}}{\lambda_{fl}} \frac{(\rho C)_{pr}}{(\rho C)_{fl}} \right)} \tag{8}$$

$$\Sigma = \frac{(1-\phi)^{-2.5} \left((1-\phi) + \phi \frac{(\rho C)_{pr}}{(\rho C)_{fl}} \right)}{\frac{\lambda_{nmf}}{\lambda_{fl}} \left((1-\phi) + \phi \frac{\rho_{pr}}{\rho_{fl}} \right)} \tag{9}$$

$$C_F = \frac{1.75}{\sqrt{150} \varepsilon^3}, \quad \bar{\lambda} = \frac{\lambda_{nmf}}{\lambda_{nmf}^*}, \quad \Lambda = \frac{\bar{\mu}}{\mu_{nmf}}$$

$$k_{nmf}^* = \frac{\lambda_{nmf}^*}{(\rho C)_{nmf}}, \quad \lambda_{nmf}^* = \varepsilon^* \lambda_{nmf} + (1-\varepsilon) \lambda_S \tag{10}$$

In the preceding equations, the dimensionless

numbers are:

$$Pr_{fl} = \frac{\mu_{fl}}{\rho_{fl} k_{Th}}, \quad Ra_{Th} = \frac{\rho_{fl} g \beta_{Th} Q R^4}{\mu_{fl} k_{Th} \lambda_{fl}}, \quad Da = \frac{K}{R^2}$$

$$Ha = RB \sqrt{\frac{\sigma_{fl}}{\mu_{fl}}}, \quad N = \frac{1}{Le} \frac{Ra_{SL}}{Ra_{fl}}, \quad Le = \frac{k_{Th}}{k_{SL}}$$

The nanofluid's thermophysical properties which depend on the fluid base and the NPs thermophysical properties are expressed as Mahian *et al.* (2013):

$$\rho_{mf} = (1 - \phi)\rho_{fl} + \phi\rho_{pr} \quad (11)$$

$$(\rho\beta)_{mf} = (1 - \phi)(\rho\beta)_{fl} + \phi(\rho\beta)_{pr} \quad (12)$$

$$(\rho C_p)_{mf} = (1 - \phi)(\rho C_p)_{fl} + \phi(\rho C_p)_{pr} \quad (13)$$

The nanofluid's dynamic viscosity is given by Brinkman (1952):

$$\mu_{mf} = \mu_{fl} (1 - \phi)^{2.5} \quad (14)$$

The nanofluid's thermal and electrical conductivity expressed, by using the Maxwell equations, as Maxwell (1904):

$$\frac{\lambda_{mf}}{\lambda_{fl}} = \frac{\lambda_{pr} + 2\lambda_{fl} + 2\phi(\lambda_{pr} - \lambda_{fl})}{\lambda_{pr} + 2\lambda_{fl} - \phi(\lambda_{pr} - \lambda_{fl})} \quad (15)$$

$$\frac{\sigma_{mf}}{\sigma_{fl}} = 1 + \frac{3\left(\frac{\sigma_{pr}}{\sigma_{fl}} - 1\right)\phi}{\left(\frac{\sigma_{pr}}{\sigma_{fl}} + 2\right) - \left(\frac{\sigma_{pr}}{\sigma_{fl}} - 1\right)\phi} \quad (16)$$

Table 1 Water and Al₂O₃ thermo-physical properties Trodi *et al.* (2017).

Property	Water	Al ₂ O ₃
ρ [Kg.m ⁻³]	0.9971*10 ³	3.970*10 ³
C_p [J.Kg ⁻¹ .K ⁻¹]	4.179*10 ³	0.765*10 ³
λ [W.m ⁻¹ .K ⁻¹]	0.613	40
β [K ⁻¹]	21*10 ⁻⁵	0.85*10 ⁻⁵

The boundary conditions, with dimensionless terms, for the considered model are:

On the inner cylinder:

$$\frac{\partial T}{\partial r} = -\frac{\lambda_{fl}}{\lambda_{mf}}, \quad \frac{\partial T}{\partial r} = 0, \quad C=1$$

$$\Psi = \frac{\partial \Psi}{\partial r} = \frac{\partial \Psi}{\partial z} = 0$$

$$\Omega = \frac{2}{\Delta r^2} \Psi \Big|_{r=1+\Delta r}$$

On the external cylinder:

$$T=0, C=0$$

$$\Psi = \frac{\partial \Psi}{\partial r} = \frac{\partial \Psi}{\partial z} = 0$$

$$\Omega = \frac{2}{\Delta r^2} \Psi \Big|_{r=AR_r-\Delta r}$$

On the bottom wall:

$$\frac{\partial T}{\partial z} = 0, \quad \frac{\partial C}{\partial z} = 0$$

$$\Psi = \frac{\partial \Psi}{\partial r} = \frac{\partial \Psi}{\partial z} = 0$$

$$\Omega = \frac{1}{r} \frac{2}{\Delta z^2} \Psi \Big|_{z=\Delta z}$$

On the top wall:

$$\frac{\partial T}{\partial z} = 0, \quad \frac{\partial C}{\partial z} = 0$$

$$\Psi = \frac{\partial \Psi}{\partial r} = \frac{\partial \Psi}{\partial z} = 0$$

$$\Omega = \frac{1}{r} \frac{2}{\Delta z^2} \Psi \Big|_{z=AR_z-\Delta z}$$

The Nusselt and Sherwood local numbers are given by Seyyedi *et al.* (2015):

$$Nu_{local} = AR_r \frac{\lambda_{mf}}{\lambda_{fl}} \frac{1}{T} \Big|_{heat_flux} \quad (17)$$

$$Sh_{local} = AR_r \frac{\partial C}{\partial r} \Big|_{inner_cylinder} \quad (18)$$

The Sherwood and Nusselt average numbers are given by:

$$Nu_{aver} = \frac{1}{\gamma} \int_0^\gamma Nu_{local} dz \quad (19)$$

$$Sh_{aver} = \int_0^1 Sh_{local} dz \quad (20)$$

3. NUMERICAL PROCEDURE OF SOLUTION

The numerical approach of systems governing the problems of natural convection seems to be essential. Firstly, because of the complexity of these problems (analytical solution seems to be impossible, except for simple problems), on the other hand to complete the experimental studies in the area.

The coupled nonlinear partial differential equations are solved by using the ADI (Alternating Direction Implicit) procedure in conjunction with finite difference approximation Sammouda *et al.* (2013). The central difference scheme is used to approximate the diffusion terms with upwind difference scheme for the convective terms. While the stream functions equation is solved by the means of S.O.R (Successive over Relaxation) procedure.

For the velocity components, the central difference approximation is used to evaluate the dynamic field at every grid point.

An irregular distribution of grid system in the radial direction in conjunction with uniform distribution

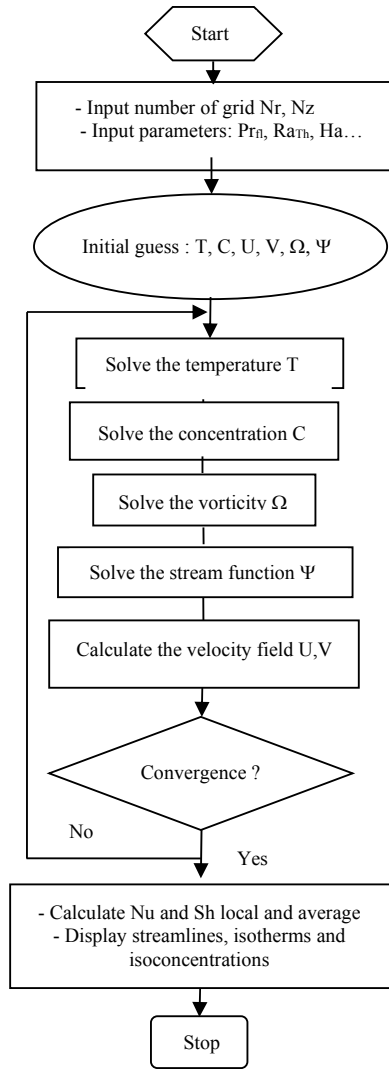


Fig. 2. Flow chart for the numerical procedure of solution.

of grid system in the axial direction is employed. To take into account the boundary effect, the mesh is refined near to the wall and especially near to the active wall. The exponential variation function is employed to generate the refined mesh grid near to the wall.

The computational procedure followed is first to solve the energy or concentration equation, which provides the temperature or concentration field necessary for the solution of the transport equation of the vorticity which itself necessary to solve the equation of stream function. The flow chart of the numerical method of solution is presented in the Fig. 2. The iteration process was employed until the maximum relative change in all dependent variables satisfies;

$$\frac{\sum \sum |F_{i,j}^{n+1} - F_{i,j}^n|}{\sum \sum |F_{i,j}^{n+1}|} \leq 10^{-5}$$

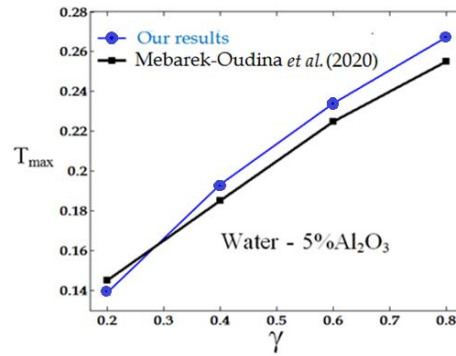
Where F refers to temperature (T), concentration (C) and vorticity (Ω), and n denotes the numbers of time steps.

Table 2 shows an accuracy test using the finite difference method using different mesh grids combinations. The present FORTRAN code is tested for grid mesh independency by calculating T_{max} . It is found that a grid size of 61×121 ensures a grid independency solution.

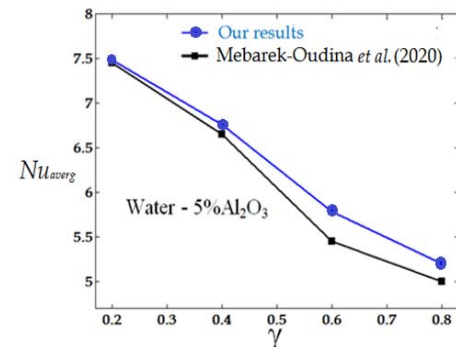
The current FORTRAN code is checked by comparing the numerical results obtained with the numerical results obtained by [Mebarek-Oudina et al. \(2020\)](#) and the [experimental data obtained by Suhil et al. \(2020\)](#).

Table 2 Comparison of T_{max} for different mesh grid solution at $Da=0.01$, $N=1$, $Le=1$, $Ha=0$, $Ra_{Th}=10^4$, $\phi=0.05$ and $\varepsilon=0.4$

Mesh size	T_{max}
21×41	0.159
31×61	0.154
41×81	0.152
51×101	0.149
61×121	0.148
71×141	0.148



(a)



(b)

Fig. 3. Effect of the heat source length on its maximum temperature (a) and the average Nusselt number (b) for $Ra_{Th}=10^4$, $Da=10^{-2}$.

4. RESULTS AND DISCUSSION

The annular space inside two cylinders with radius ratio (R_e/R_i) equal to 2 and aspect ratio (H/R_i) equal to 2 has been considered for this simulation studies. At lower temperatures and concentrations, the outer cylinder is sustained, the discrete heat flux with the unheated adiabatic sections as well as the higher concentration are imposed at the inside wall of the central cylinder. The base walls are insulated and impermeable. In the vertical direction, external MF with constant intensity is applied. The dimensionless length ratio of the heat flux ($\gamma = 0.4$). The considered nanofluid is Newtonian, incompressible and obeys to the Boussinesq approximation. Water is used as base fluid ($Pr_{fl} = 6.2$). Table.1. reports the properties of the mixture (water- Al_2O_3). The NPs volume fraction range is ($\phi = 0.05-0.1$).

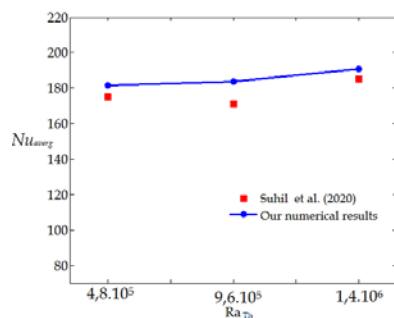


Fig. 4. Comparison of our numerical results to experimental results of Suhil et al. (2020).

The obtained results of the numerical simulation, presented in terms of concentration and temperature distributions inside the enclosure, streamlines, Nu_{local} , Nu_{avg} , Sh_{local} and Sh_{avg} are represented to show the effects of Ra_{Th} , Ha numbers, N and the solid NPs volume fraction on the fluid flow pattern, the scalar field of concentration and temperature inside enclosure as well as the transferred mass and thermal energy.

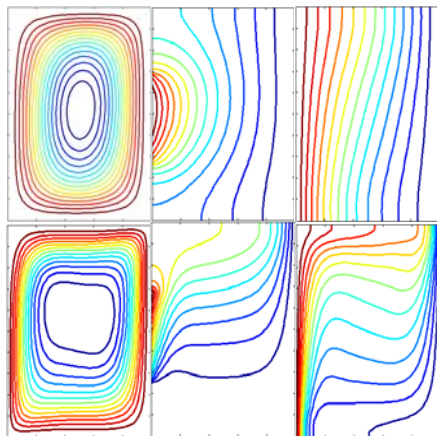


Fig. 5. Streamlines, isotherms and isoconcentrations for $N=1$, $Ha=0$, $Da=0.01$, $Pr_{fl}=6.2$, $\phi=0.05$ and $Ra_{Th}=10^3$ (top) $Ra_{Th}=10^5$ (bottom).

Figure 5 represents streamlines, temperature and concentration distributions inside enclosure for the mixture (water- Al_2O_3) with NPs volume fraction $\phi = 0.05$ and for various values of Ra_{Th} . As exposed in this figure, for low values of number of Ra_{Th} ($Ra_{Th}=2.10^3$), one clockwise circular cell filling the entire enclosure illustrates the fluid flow. The concentration distributions are almost straight, dispersed inside the whole enclosure. We can see that the temperature distributions are curved in the region of the heat source and are almost straight near to the cold wall. The intensity of circulation of the nanofluid increases as Ra_{Th} increases for large values; this contributes to an improvement in the transport of mass and thermal energy due to increased convection. The concentration distributions are compressed in the bottom walls of the inner cylinder and the top walls of the outer cylinder. The temperature distributions are compressed in the two sides of heat source which signify the presence of important gradients in temperature due to a significant heat transfer by convection in these areas. In fact, the increase of Ra_{Th} causes the increase of buoyancy forces which leads to an improvement of mass and thermal energy transport in the active walls.

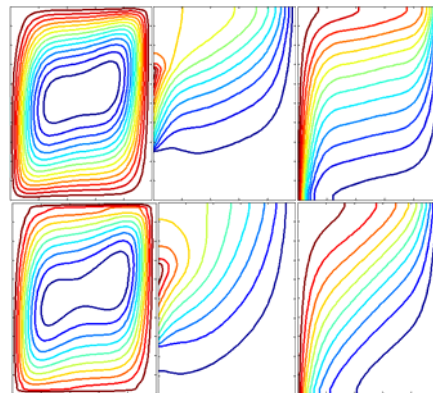


Fig. 6. Streamlines, isotherms and isoconcentrations for $N=1$, $Ra=10^5$, $Da=0.01$, $Pr=6.2$, $\phi=0.05$ and $Ha=50$ (top) $Ha=150$ (bottom).

The temperature and concentration distributions with streamlines for range values of Ha number are exposed in the Fig.6 to illustrate the MF intensity effect on the pattern of nanofluid flow and the rate of mass and thermal energy transferred in the active walls. As seen in the figure, the temperatures and concentration distributions are influenced, when Ha increases. The concentration distributions becomes almost straight, the temperatures distributions becomes less curved and almost straight far from the heat flux. This behavior indicates that for higher Ha values, the strength of the fluid flow circulations become weak. It can be explained by the fact that is the consequence of Lorentz force. Indeed, the increase of the intensity of the external MF decreases the intensity of fluid flow circulation. This simply means that the conduction mode

becomes dominant in the convection mode as Ha increases.

Figure 7 represents temperature and concentration distributions and streamlines for mixture (water- Al_2O_3) with NPs volume fraction $\phi = 0.05$ and various values of N and Ha numbers to illustrate their consequence on the strength of fluid circulation and the rate of the mass and the thermal energy transport on the active walls. As seen in the figure, for negatives values of the ratio of buoyancy forces, one clockwise circular cell filling the entire enclosure illustrates the fluid flow. The concentration distributions are almost straight, which means that the conduction mode is dominant to convection mode. As N number increases for negatives values, the intensity of fluid circulation of the cell becomes more important. The transferred heat and mass rate is more important in this case. The same observation is made, in this case, when we increase the Ha number, the intensity of nano-fluid flow circulation becomes weak, and the conduction mode is dominant.

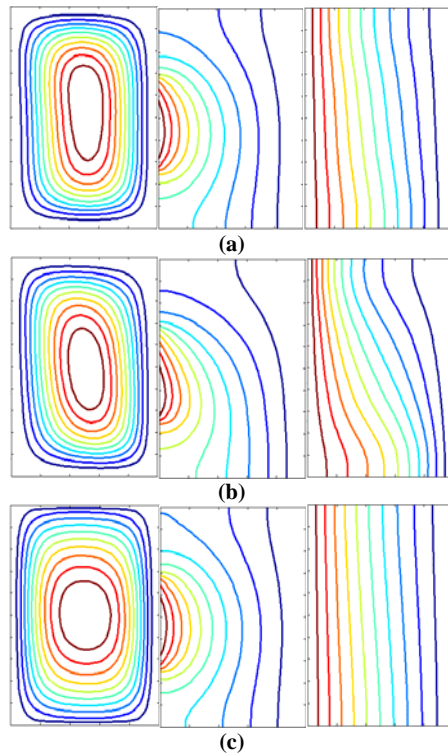


Fig. 7. Streamlines, isotherms and isoconcentrations for $Ra_{Th}=10^3$, $Da=0.01$, $Pr_f=6.2$, $\phi=0.05$ and $(Ha=0, N=-1(a)), (Ha=0, N=-3 (b)), (Ha=100, N=-3 (c)).$

Figure 8 and Figure 9 represents the variations of Nu_{loc} and Sh_{loc} along the heat flux and at the central cylinder respectively for various numbers of Ra_{Th} , without and with MF respectively. As seen in the figure, the local heat transport in terms of Nu_{loc} and local mass transport in term of Sh_{loc} are observed to increase with the Ra_{Th} number increase

Fig.8. It's also observed that the rate of the mass and the thermal energy transport along the heat flux and at the external wall of the cylinder put in the middle respectively decreases as Ha number increases. With high values of Ha number, the conduction mode is dominant.

Figure 10 represents the Nu_{avg} and Sh_{avg} variations along the heat flux and at the central cylinder respectively, for various Ha numbers and for diverse values of the NPs volume fraction.

The Nu_{avg} and Sh_{avg} decreases as Ha number increases. It is also noticed that with the increase in the NPs volume fraction of (water- Al_2O_3) nanofluid, the Nu_{avg} number increases, but the Sh_{avg} declining. The addition of NPs has an effect on the rate of the mass and the thermal energy transport. This addition of the solid NPs increases the rate of heat transport and reduces the rate of mass transfer due to the decrease in the intensity of fluid circulation.

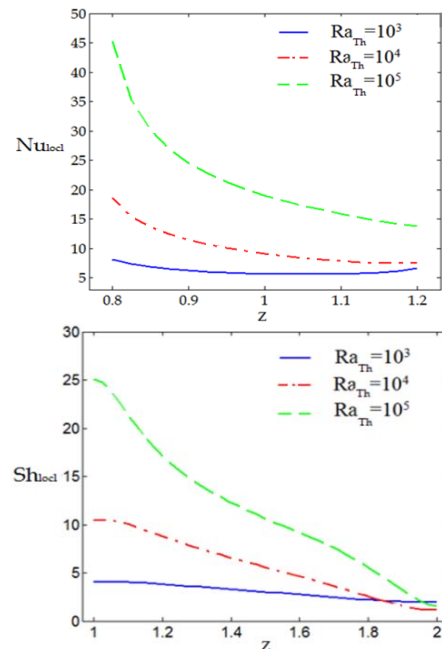


Fig. 8. Rayleigh effect on local Nusselt (source) and Sherwood numbers for $Da=0.01$, $N=1$, $Pr_f=6.2$, $\phi=0.05$ and $Ha=0$.

Figure 11 represents the Nu_{avg} and Sh_{avg} variations along the heat flux and at the central cylinder respectively, for various values of N and NPs volume fraction. As seen in the figure, the Nu_{avg} increases as the NPs volume fraction of (water- Al_2O_3) nanofluid increases, but the Sh_{avg} declining. We can clearly see also that, the rate of the mass and thermal energy transport increases with the increase of N , in absolute values. The rate of mass and thermal energy transport is further improved for positive values of N . Indeed, the solutal and thermal buoyancy forces are opposed, for negatives N values, the intensity of fluid flow circulation decreases rendering the mass and the thermal energy transfer frail.

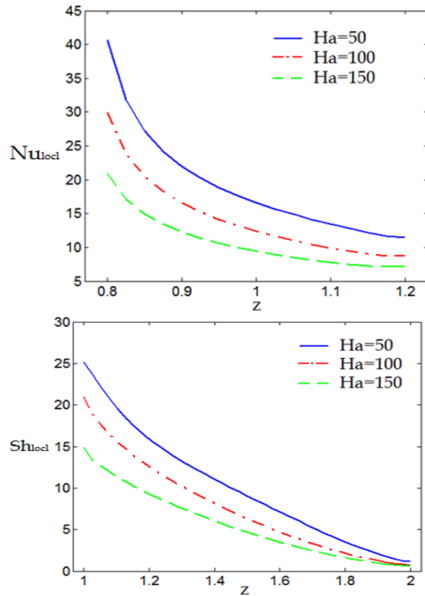


Fig. 9. Ha effect on local Nusselt (source) and Sherwood numbers for $Da=0.01$, $N=1$, $Pr_f=6.2$, $\phi=0.05$ and $Ra_{Th}=10^5$.

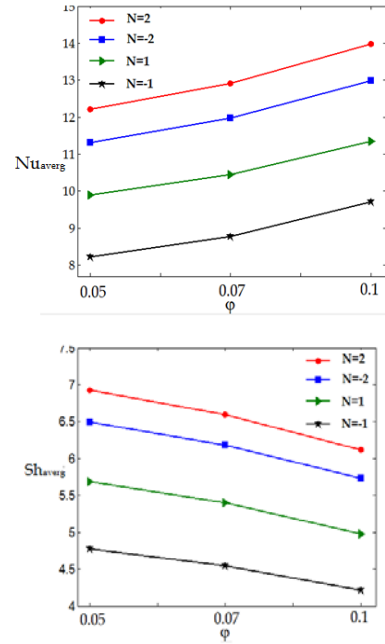


Fig. 11. Variation of average Nusselt number (source) and Sherwood number for $Da=0.01$, $Ha=0$, $Pr_f=6.2$, and $Ra_{Th}=10^4$.

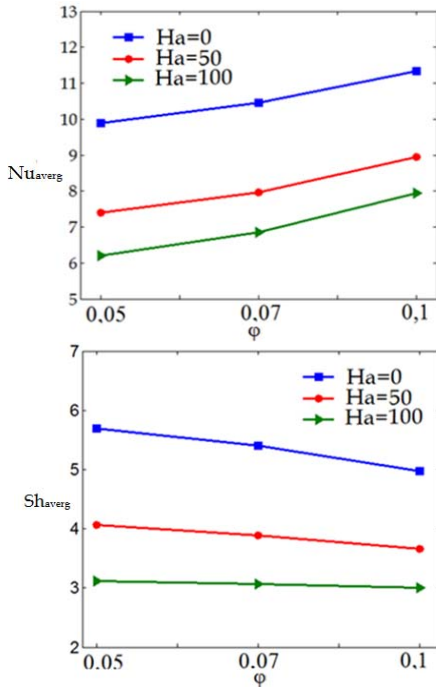


Fig. 10. Variation of average Nusselt number (source) and Sherwood number for $Da=0.01$, $N=1$, $Pr_f=6.2$, and $Ra_{Th}=10^5$.

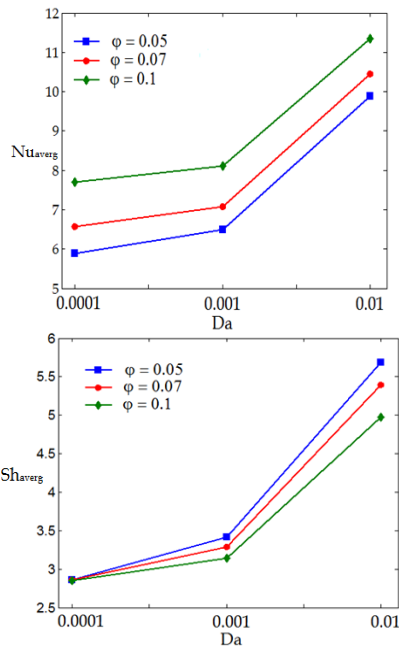


Fig. 12. Variation of average Nusselt number (source) and Sherwood number for $N=1$, $Ha=0$, $Pr_f=6.2$, and $Ra_{Th}=10^4$.

The effect of Da number and the solid NPs volume fraction on the mass and the thermal energy transport in terms of Nu_{avg} and Sh_{avg} along the heat flux and on the outer walls of the cylinder placed in the middle respectively, are exhibited in Fig. 12. The rate of the mass and the thermal energy transport increases as anticipated with the growth of

the Da number. Indeed, the permeability of porous medium increases as Da number increases rendering the intensity of nanofluid flow circulation and the rate of the mass and the thermal energy transport increases. We can see also from this figure that the Nu_{avg} increases with the NPs volume fraction but the Sh_{avg} declining. For low values of

Da there is no consequence of the NPs volume fraction on Sh_{avg} number.

5. CONCLUSION

In the current study, the phenomenon of MHD thermosolutal convection in an annular space inside two concentric cylinders charged with a saturated porous matrix by (Al_2O_3 - water) Newtonian nanofluid and exposed to a constant heat flux and a constant intensity of MF has been numerically investigated. The influence of MF, heat flux and the ratio of thermal and solutal buoyancy forces on the flow pattern and the rate of the mass and thermal energy transferred near to the active walls have been studied in detail. To induce the natural convection, at lower temperature and concentration, the outer cylinder is sustained, the discrete heat flux with the unheated adiabatic portions as well as the higher concentration are imposed in the central cylinder. The base walls are insulated and impermeable. In the vertical direction, external MF of uniform intensity is applied.

The problem has been solved numerically using the finite difference method. The obtained results of the numerical simulation are presented in terms of temperature and concentration distributions, streamlines, Nu_{loc} , Nu_{avg} , Sh_{loc} and Sh_{avg} numbers for wide ranges of principal parameters. The following conclusions are drawn:

The intensity of nanofluid flow circulation augments with the growth of Rayleigh number Ra_{Th} , the ratio of thermal and solutal buoyancy forces N , and Darcy number Da , while it decreases with increasing the Hartmann number and the solid NPs volume fraction.

The rate of thermal energy transferred in the active wall increases with the growth of solid NPs volume fraction, while the rate of mass transport decreases.

For low values of Darcy number Da , there is no consequence of the NPs volume fraction on the rate of mass transport.

The mass and thermal energy transport in active wall is further improved for positive values of buoyancy ratio N than for negative values.

The greater magnetism declines the rate of the mass and thermal energy transport. This shows that the MF has a stabilizing effect on the nanofluid flow.

REFERENCES

- Ahmad, S., M. Ashraf and K. Ali (2020). Nanofluid Flow Comprising Gyrotactic Microorganisms through a Porous Medium. *Journal of Applied Fluid Mechanics* 13(5), 1539-1549.
- Brinkman, H. C. (1952). The viscosity of concentrated suspensions and solution. *Journal. Chem. Phys* 20, 5171-5181.
- Cheng, C. Y. (2009). Natural convection heat and mass transfer from a vertical truncated cone in a porous medium saturated with non-Newtonian fluid with variable wall temperature and concentration. *International Communication in Heat and Mass Transfer* 36, 585-589.
- Dat, D. V., M. Hedayat, T. Ambreen, S. A. Shehzad, M. Sheikholeslami, A. Shafee and T. K. Nguyen (2019). Effectiveness of various shapes of Al_2O_3 nanoparticles on the MHD convective heat transportation in porous medium. *Journal of Thermal Analysis and Calorimetry* 139, 1345-1353.
- Donald A. and A. B. Nield (2006). *Convection in Porous Media*. Third Edition. New York, USA.
- Fakour, M., D. D. Ganji, A. Khalili and A. Bakhshi (2017). Heat transfer in nanofluid MHD flow in a channel with permeable walls. *Heat Transfer Research* 48(3), 221-238.
- Ghorayeb, K. and M. Abdelkader. (1997). Double diffusive convection in a vertical rectangular cavity. *Physics of Fluids* 9(8), 2339-2348.
- Hemmat Esfe, M., A. H. Refahi, H. Teimouri, M. J. Noroozi, M. Afrand and A. Karimiopour. (2015). Mixed convection fluid flow and heat transfer of the Al_2O_3 -Water nanofluid with variable properties in a cavity with an inside quadrilateral obstacle. *Heat Transfer Research* 46(5), 465-482, 2015.
- Jagadeesha, R. D., B. M. R. Prasanna and M. Sankar (2015). Double Diffusive Convection in an Inclined Parallelogrammic Porous Enclosure. *Procedia Engineering* 127, 1346-1353.
- Jagadeesha, R. D., B. M. R. Prasanna and M. Sankar (2017). Numerical simulation of double diffusive magnetoconvection in an inclined parallelogrammic porous enclosure with an internal heat source. *In Proceedings of International Conference on Recent Trends in Engineering and Material Sciences, Jaipur, India* 4(9), 10544-10548.
- Kaviany, M. (1995) *Principles of Heat Transfer in Porous Media*. Second Edition. New York, USA
- Kramer, J. (2007). Boundary domain integral method for the study of double diffusive natural convection in porous media. *Engineering Analysis with Boundary Elements* 31, 897-905.
- Luzia, A., T. Marcelo and J. S. de Lemos (2009). Double diffusive turbulent natural convection in a porous square cavity with opposing temperature and concentration gradients. *International Communication in Heat and Mass Transfer* 36, 991-995.
- Mahapatra, T. R., C. Bikash and D. P. Saha (2018). Magnetohydrodynamic double-diffusive

- natural convection for nanofluid within a trapezoidal enclosure. *Computational and Applied Mathematics* 37(5), 6132–6151.
- Mahian, O., A. Kianifar, C. Kleinstreuer, M. A. Al-Nimr, I. Pop, A. Z. Sahin and S. Wongwises (2013). A review of entropy generation in nanofluid flow. *International journal of Heat and Mass Transfer* 65, 514–532.
- Maxwell, J. C. and A Treatise (1904) on *Electricity and Magnetism*, Second Edition. *Oxford University Press, Cambridge*.
- Mebarek-Oudina, F. and R. Bessaih (2016). Oscillatory magnetohydrodynamic natural convection of liquid metal between vertical coaxial cylinders, *Journal of Applied Fluid Mechanics* 9(4), 1655–1665.
- Mebarek-Oudina, F., A. Aissa, B. Mahanthesh, and K.F. Oztop (2020). Heat transport of magnetized Newtonian nanofluids in an annular space between porous vertical cylinders with discrete heat source. *International Communications in Heat and Mass Transfer* 117, 104737.
- Mohebbi, R., S. Haghghi Khalilabad and Ma, Y. (2019). Effect of γ -Al₂O₃/Water Nanofluid on Natural Convection Heat Transfer of Corrugated Shaped Cavity: Study the Different Aspect Ratio of Grooves. *Journal of Applied Fluid Mechanics* 12(4), 1151-1160.
- Muthtamilselvan, M., K. Periyadurai and H. D. Deog (2018). Impact of non uniform heated plate on double-diffusive natural convection of micropolar fluid in a square cavity with Soret and Dufour effects. *Advanced Powder Technology*, 29 (1), 66-77.
- Rujda, P. and T. R. Mahapatra (2019). Numerical simulation of MHD double diffusive natural convection and entropy generation in a wavy enclosure filled with nanofluid with discrete heating. *Heliyon* 5, e02496.
- Saini, S. and Y. D. Sharma (2018). Double-Diffusive Bioconvection in a Suspension of Gyrotactic Microorganisms Saturated by Nanofluid. *Journal of Applied Fluid Mechanics* 12(1), 271-280.
- Sammouda, M. K. Gueraoui, M. Driouich, M. Ghoulil and A. Dhiri (2013). Double diffusive natural convection in Non-Darcy porous media with Non-uniform porosity. *International Review of Mechanical Engineering* 7(6), 1021-1030.
- Sammouda, M., K. Gueraoui, M. Driouich, A. El Hammoumi and A. Iben Brahim (2011). The variable porosity effect on the natural convection in a Non-Darcy porous media, *International Review on Modelling and Simulations* 4(5), 2701-2707.
- Sarлак, S., S. Yousefzadeh, O. Ali Akbari, D. Toghraie, R. Sarлак and F. Assadi (2020). Numerical investigation of MHD mixed convection of water-CuO nanofluid in a square enclosure with vortex generators in different arrangements. *Heat Transfer Research* 51(6), 571–601.
- Seyyedi, S. M., M. Dayyan, Soleimani, S. and E. Ghasemi (2015). Natural convection heat transfer under constant heat flux wall in a nanofluid filled annulus enclosure. *Ain Shams Engineering Journal* 6, 267–280.
- Shahid, H. and M. Altamush Siddiqui (2016). Experimental and numerical analyses of natural convection flow in a partially heated vertical annulus. *Numerical Heat Transfer, Part A: Applications* 70(7), 763-775.
- Sivasanka, S. and P. Kandaswami (2008). Double diffusive convection of anomalous density fluids in a porous cavity. *Transport in Porous Media* 71, 133-145.
- Sohankar, A., M. Riahi and E. Shirani (2019). Numerical Study of Water/Al₂O₃ Nanofluid Forced Convection in a Rotating Hydrophilic and Hydrophobic Microchannel. *Journal of Applied Fluid Mechanics* 12(1), 219-231.
- Suhil, K., H. Alwan and N. Abdelal. (2020). An experimental investigation of the natural convection heat transfer from a vertical cylinder using porous fins. *Applied Thermal Engineering* 179, 115673.
- Tapas, R., D. P. Mahapatra and M. Sabyasachi, (2013). Effects of buoyancy ratio on double-diffusive natural convection in a lid-driven cavity. *International Journal of Heat and Mass Transfer* 57, 771–785.
- Trodi, A. and B. Mohammed El Hocine (2017). Particle Shape and Aspect Ratio Effect of Al₂O₃–Water Nanofluid on Natural Convective Heat Transfer Enhancement in Differentially Heated Square Enclosures, *Chemical Engineering Communications* 204(2), 158-167.
- Trung, N. T., M. Sheikholeslami, Z. Shah, P. Kumam and A. Shafee (2019). Magnetohydrodynamic nanofluid radiative thermal behavior by means of Darcy law inside a porous media. *Scientific Reports* 9, 12765.
- Yadav, D. and J. Wang (2018). Convective Heat Transport in a Heat Generating Porous Layer Saturated by a Non-Newtonian Nanofluid. *Heat Transfer Engineering* 40(16), 1363-1382.
- Yadav, D., J. Wang and J. Lee, (2017). Onset of Darcy-Brinkman convection in a rotating porous layer induced by purely internal heating. *Journal of Porous Media* 20(8), 691–706.
- Yadav, D., J. Wang, J. Lee and H. H. Cho (2016). Numerical investigation of the effect of magnetic field on the onset of nanofluid convection. *Applied Thermal Engineering* 103, 1441-1449.